Downes, Hilary and de Vries, C. and Wittig, N. (2015) Hf–Zr anomalies in clinopyroxene from mantle xenoliths from France and Poland: implications for Lu–Hf dating of spinel peridotite lithospheric mantle. International Journal of Earth Sciences 104 (1), pp. 89-102. ISSN 1437-3254.

Hf-Zr anomalies in clinopyroxene from mantle xenoliths from France and Poland: implications for Lu-Hf dating of spinel peridotite lithospheric mantle

Hilary Downes[1], Caja de Vries[1] and Nadine Wittig[2]

1. Department of Earth and Planetary Sciences, Birkbeck University of London, Malet Street London WC1E 7HX UK.

2. Department of Earth Sciences, Carleton University, Ottawa, Ontario, K1S 5B6 Canada

ABSTRACT

Clinopyroxenes in some fresh anhydrous spinel peridotite mantle xenoliths from the northern Massif Central (France) and Lower Silesia (Poland), analysed for a range of incompatible trace elements by Laser Ablation-Inductively Coupled Plasma Mass Spectometry, show unusually strong negative anomalies in Hf and Zr relative to adjacent elements Sm and Nd, on primitive-mantle-normalised diagrams. Similar Zr-Hf anomalies have only rarely been reported from clinopyroxene in spinel peridotite mantle xenoliths worldwide, and most are not as strong as the examples reported here. Low Hf contents give rise to a wide range of Lu/Hf ratios, which over geological time would result in highly radiogenic εHf values, decoupling them from εNd ratios. The high $^{176}Lu/^{177}Hf$ could in theory produce an isochronous relationship with $^{176}Hf/^{177}Hf$ over time; an errorchron is shown by clinopyroxene from mantle xenoliths from the northern Massif Central. However, in a review of the literature, we show that most mantle spinel peridotites do not show such high Lu/Hf ratios in their constituent clinopyroxenes, because they lack the distinctive Zr-Hf anomaly, and this limits the usefulness of the application of the Lu-Hf system of dating to garnet-free mantle rocks. Nevertheless, some mantle xenoliths from Poland or the Czech Republic may be amenable to Hf-isotope dating in the future.

Keywords: mantle, spinel peridotite, clinopyroxene, France, Poland, Lu-Hf geochronology

1. DATING EVENTS WITHIN THE UPPER MANTLE

Methods have long been sought that can date events which have occurred within the shallow (spinel peridotite) subcontinental lithospheric mantle. Success has been achieved in those rare mantle rocks that contain zircon (e.g. Sanchez-Rodriguez and Gebauer 2000; Femenias et al., 2003; Zheng et al., 2006), probably related to enrichment in the lithosphere by silicate melts. Osmium isotope methods based on model ages or Re-depletion ages can provide a guide to the age of mantle events (e.g. Pearson et al., 2002; Schmidt and Snow, 2002; Handler et al., 2003; Widom et al., 2003; Xu et al., 2008; Rudnick and Walker, 2009; Janney et al., 2010; Wittig et al., 2010a; Wittig et al., 2010b) but are best applied to regions of ancient lithospheric mantle. The Sm-Nd isotope system can be used to determine model ages, but this system is strongly affected by mantle metasomatism, leading to mixed ages that are probably meaningless (Zangana, 1995). Notable exceptions are the "approximate isochron" shown by clinopyroxenes from mantle xenoliths from Inner Mongolia (Deng and Macdougall, 1992) and errorchrons shown by minerals from mantle spinel peridotite xenoliths from Jordan (Nasir and Rollinson, 2009).

In contrast, the Lu-Hf system may provide a more robust method of dating mantle lithologies, particularly of garnet peridotites, garnet pyroxenites and eclogites (e.g., Schmidberger et al., 2002, 2007; Ionov 2004; Lazarov et al., 2009; Gonzaga et al., 2010; Shu et al., 2013). Its decay scheme (^{176}Lu decays to ^{176}Hf with decay constant of 1.865 x 10^{-11} yr^{-1} (Scherer et al., 2001; Söderlund et al., 2004)) is suitable for dating ancient mantle events, and it is less prone to respond to metasomatism, because many potential metasomatic agents have low Lu and Hf contents. Since Lu is a heavy rare earth element, it shows greater compatibility with the mantle compared to Hf, which has a compatibility similar to that of Sm and Nd during mantle melting. The question then arises as to whether Lu-Hf isotopic system could be appropriately applied to garnet-free mantle peridotite samples.

Clinopyroxene is the main host of most incompatible lithophile trace elements in the garnet-free anhydrous lithospheric mantle. Dobosi et al (2010) has shown in a study of Pannonian Basin mantle peridotite xenoliths that the abundances of incompatible trace elements in mantle clinopyroxenes are usually much greater (by an order of magnitude or more) than those in coexisting orthopyroxenes, and that the abundances of Lu, Hf, Zr, Sm and Nd in clinopyroxene always exceed those in orthopyroxene. Hence for technical reasons, it is not possible to use the other minerals in a mantle xenolith to derive an internal mineral isochron.

Figure 1 shows a compilation of Lu/Hf and Sm/Nd ratios from clinopyroxenes in mantle spinel peridotites worldwide. It demonstrates that the range of Lu/Hf ratios reported for mantle clinopyroxenes is much greater than the range in Sm/Nd. There is a “common mantle clinopyroxene” field with Sm/Nd ratios of 0.2-0.4 and Lu/Hf ratios of 0.1-0.3. This field is centered on the value for Lu/Hf and Sm/Nd in primitive mantle (Sun and McDonough1989). However, in other mantle samples, Sm/Nd ratios in clinopyroxene rarely exceed 0.7 whereas Lu/Hf ratios greater than 1 are not unknown. Thus Hf model ages and Lu-Hf isochrons might theoretically be derived from these garnet-free samples that have experienced depletion events and were not overwritten by metasomatic addition of Lu or Hf to the lithospheric mantle. In this study, we report the trace element compositions of clinopyroxenes in a variety of four-phase anhydrous mantle spinel peridotite xenoliths from France and SW Poland that show a wide range of Lu/Hf ratios, resulting from variable depletion in Hf. We compare them to clinopyroxenes from mantle spinel peridotites worldwide and show that only a very small proportion of clinopyroxenes in garnet-free mantle rocks have experienced sufficient fractionation of Hf from Lu to be amenable to dating by this method.

2. METHODOLOGY AND SAMPLES ANALYSED

Forty-three spinel peridotite mantle xenoliths from Neogene alkali basalts of the French Massif Central were analysed. Petrological details, sample localities and major element compositions have been discussed extensively elsewhere (Downes and Dupuy 1987; Zangana et al., 1998; Downes et al., 2003). They are all Cr-diopside and contain no hydrous minerals. Clinopyroxene from xenoliths from the northern domain have lower TiO_2 and Na_2O contents (<0.5 wt% and <1.2 wt%, respectively) than those from the southern domain (Downes et al., 2003), suggesting more extensive depletion in the northern domain mantle. Trace element abundances in clinopyroxenes from some of these samples had been analysed previously by different methods and in different laboratories (Downes and Dupuy 1987; Vannucci et al., 1994; Zangana et al., 1998; Mason et al., 1999; Downes et al., 2003). Clinopyroxene grains were hand-picked from these samples, usually from the medium grain size fraction (850-425 μm). In addition, separated clinopyroxene from sixteen spinel peridotite mantle xenoliths from the Neogene alkali basalts in the Polish Sudetes (Lower Silesia – localities Ladek, Lutynia and Wilcza Gora) were provided by Dr J Blusztajn and correspond to the samples previously described by Blusztajn and Shimizu (1994). These clinopyroxene are also Cr-diopsides and have low TiO_2 and Na_2O contents similar to those of the Northern Massif Central domain. Similar material has been studied more recently by Matusiak-Malekj et al (2010) and Puziewicz et al. (2011). Up to eight grains per sample were analysed, with a minimum of 3 points per grain; the results were averaged for each sample. No differences between cores and rims were detected.

Trace element compositions were determined by in situ laser ablation inductively coupled plasma mass spectrometry (LA-ICPMS) at Birkbeck/UCL. The analytical instrumentation consists of a New Wave Research YP213 laser aperture imaged frequency quintupled Nd:YAG solid state laser source, operating at a wavelength of 213 nm, coupled to an Agilent 7500a quadrupole ICP-MS. A 50 micron laser spot size was used. Time-resolved analysis was employed during data acquisition. The samples were ablated with pulses of 80mJ at a pulse repetition rate of 5Hz, over an ablation time of 20 s. The synthetic glass reference material NIST 612 was used as a calibration standard with the average composition of Pearce et al. (1997). Ca contents of clinopyroxenes analysed by electron microprobe were used for internal calibration to correct for differences in ablation characteristics between samples and standards. The GEMOC Glitter reduction software was used to process the raw data. This program provides minimum detection limits for all elements in each individual analysis, and the data reported were all above the relevant detection limit. Any results that were below detection limit (a common case with Rb and Ba concentrations in mantle clinopyroxenes) are shown in the Tables as a blank.

An in-house standard RP91-17, a clinopyroxene from a mantle xenolith from the southern French Massif Central (Zangana et al., 1998), was used to ensure comparability with previously determined values by LA-ICPMS (Mason et al., 1999) who also used the NIST 612 international standard. Trace element compositions of clinopyroxenes from the Massif Central are given in Table 1, together with data for the in-house standard; those for clinopyroxene from mantle xenoliths from Poland are given in Table 2. In general the comparability between our results for RP 91-17 and those of Mason et al (1999) are very good, i.e. within 1-2%, but there is a significant discrepancy for Pb concentrations (our value = 0.38 ppm; that of Mason et al (1999) is 1.5 ppm). We consider that this may be due to a memory effect in the earlier analysis, as the same standard clinopyroxene analysed using the LA-ICPMS facility at Kingston University yielded a value of 0.17 ppm Pb. Comparisons of our LA-ICPMS Lu and Hf analyses with concentrations given by Wittig et al (2006) on bulk clinopyroxenes by isotope dilution (ID) are generally good despite ID being inherently a more precise method (e.g. for sample Mb50, Lu = 0.1277 ppm by ID and 0.12 ppm by LA-ICPMS; Hf = 0.032 ppm by ID and 0.02 ppm by LA-ICPMS). Discrepancies may also be due to the different volumes of material that are analysed by the two different methods, with ID analysing much larger volume of clinopyroxene.

3. TRACE ELEMENT VARIATIONS IN CLINOPYROXENES FROM SPINEL PERIDOTITES

It has been recognized that the sub-continental mantle lithosphere beneath the French Massif Central is separated into a northern and southern domain characterized by contrasting bulk rock compositions of mantle xenoliths (Lenoir et al., 2000), clinopyroxene compositions (Downes et al., 2003) and geophysical signatures (Babuska et al., 2002). The mantle xenoliths from the Massif Central have therefore been divided into those two geographic groups, which also correspond to differences in their trace element patterns. Clinopyroxenes in xenoliths from the southern region (samples prefixed by RP, Bo, Ta, Gr, Ce, Vp, Pey, BR, Ms, AL and Z in Table 1), tend to show flat trace element patterns (Fig. 2), when normalised to primitive mantle (Sun and McDonough 1989). Their Zr/Hf ratios are mostly in the range 23 to 44, i.e. approximately chondritic (36), although a very small number of analyses have strongly sub-chondritic values (3-13). In contrast, clinopyroxenes from northern localities (Mb, PH, FR, Bt, St and CH in Table 1) tend to show highly spiked patterns, with several samples showing particularly strong negative anomalies in Zr and Hf (Fig. 2). These samples also show positive anomalies in Sr, Pb, La and U compared to adjacent elements, and strong enrichment in LREE over MREE. The Zr/Hf ratios of these unusual clinopyroxenes vary from strongly subchondritic to suprachondritic (0.5 to 82). Some of the variation may be a result of analytical problems, given that the Hf content of these minerals is conspicuously low (less than 0.05 ppm).

Clinopyroxenes from mantle xenoliths from SW Poland (Fig. 3) also show a variety of trace element patterns, although there is no clear correlation with location. Our trace element results are similar to those of Matusiak-Malek et al (2010) for different samples from similar localities. In general they are more enriched in the LREE than the Massif Central samples, and show conspicuous troughs at Ta and Pb. However, some also show conspicuous negative anomalies in Zr and Hf, although these are not as strong as those seen in mantle clinopyroxenes from the northern Massif Central. Their Zr/Hf ratios are in the range 3-151. The Polish samples appear to show significant decoupling of Ta relative to Nb. Similar low Ta values are also shown in clinopyroxenes from Polish mantle xenoliths analysed by Matusiak-Malek et al. (2010), but unfortunately Nb was not analysed in that study. Although this is beyond the scope of this paper, the superchondritic Nb/Ta values in the Polish mantle clinopyroxenes are worthy of further investigation.

Further examples of Zr-Hf-depleted clinopyroxenes have been found in spinel peridotite xenolith suites from elsewhere in Europe (Fig. 4), namely Monte Vulture in southern Italy (Downes et al., 2002), the Hyblean Plateau in Sicily (Perinelli et al., 2008) and the Bohemian massif within the Czech Republic (Ackerman et al., in press). Such strong Zr-Hf anomalies are uncommon in clinopyroxene from mantle peridotites worldwide, although other examples (Fig. 4) have been reported from peridotite xenoliths from the Bearpaw Mountains, Montana (Downes et al., 2004) and Tok, Siberia (Ionov et al., 2006). Clinopyroxene from a mantle xenolith from the Avacha volcano in Kamchatka situated above an active subduction zone (Halama et al., 2009), shows similarly low Hf abundances but does not show the same extent of Lu/Hf fractionation.

4. Hf ISOTOPE COMPOSITIONS OF CLINOPYROXENES IN SPINEL PERIDOTITES

Mantle peridotite clinopyroxenes analysed in this study display a range of Lu contents from 0.05 to 0.45 ppm, whereas their Hf contents range from 0.01 to 2.5 ppm. Worldwide mantle peridotite clinopyroxenes show similar ranges in Lu and Hf (although samples from Tok in Siberia (Ionov et al., 2006a) show even higher Hf contents, up to 5.65 ppm, that are not accompanied by high Lu contents). There is a broad but very poor positive correlation between Lu and Hf contents in mantle clinopyroxenes (not shown). Figure 5 shows the Lu/Hf ratios of our samples plotted as a function of Hf content, compared with a worldwide data set of mantle peridotite clinopyroxene compositions. We have included clinopyroxene from a mantle xenolith from Avacha volcano (Halama et al., 2009), situated above an active subduction zone, for comparison. Only clinopyroxenes that contain less than 0.1 ppm Hf show high Lu/Hf ratios, ranging from 1 to 100. A wide range of Lu/Hf ratios would be a prerequisite for dating mantle events using the Lu-Hf method. Only a suite of mantle peridotite samples that includes clinopyroxenes with high Lu/Hf ratios, such as those from the northern Massif Central, would be amenable to Lu-Hf isotopic age dating, and then only if neither Lu nor Hf had been added to the sample by later events such as metasomatism.

Methodology and results for Hf isotope compositions in clinopyroxenes from a subset of Massif Central spinel peridotite xenoliths were reported by Wittig et al. (2006, 2007). Figure 6 shows the εHf- εNd isotope diagram for clinopyroxenes from xenoliths from the northern and southern domains of the region. Those from the southern domain show relatively little variation in εHf, ranging from +5.4 to +22; εNd values range from +0.08 to +16. In contrast, samples from the northern domain show extreme values of both εHf (+140 to +2586) and εNd (+2 to +91).

The northern Massif Central xenoliths are also very different in their isotopic composition from other spinel peridotite xenoliths worldwide, as shown in Figure 7 (in which the samples from the Massif Central with the highest εHf and εNd values have been omitted, in order for the remaining data to be shown clearly on the scale). Clinopyroxenes from almost all other mantle spinel peridotites cluster in a small area of the εNd- εHf diagram (Fig. 7), near the values for Mid-Ocean Ridge Basalts and Ocean Island Basalts, whereas those from the northern Massif Central show much higher εHf values (and, more rarely, higher εNd values). Only a few samples (e.g. one each from Lherz, Jordan and Spitsbergen) show such highly radiogenic Hf isotope values. Such ultradepleted lithospheric mantle domains have been discussed by Rampone and Hofmann (2012) and Stracke et al (2011). These studies showed εHf values up to +110 for these depleted domains, which are low compared with those found in Massif Central mantle clinopyroxenes (εHf = +140 to +2586).

^{176}Hf/^{177}Hf-^{176}Lu/^{177}Hf data for clinopyroxenes from several different mantle xenoliths from the northern Massif Central (Wittig et al., 2006) form a strong correlation (Fig. 8) which has been interpreted as an errorchron with an apparent age of 344±11 Ma. Disregarding the two samples with highest values of ^{176}Hf/^{177}Hf-^{176}Lu/^{177}Hf still yields an age of 350±61 Ma. In contrast, mantle peridotites from elsewhere in the world (Schmidberger et al., 2002; Le Roux et al., 2009; Choi et al., 2010) all plot at the extremely low end of this array, as do the mantle garnet data of Lazarov et al (2009). Even the sub-calcic garnet data for garnet peridotite xenoliths from South Africa (Shu et al., 2013) plot in the low end of the array, but because of the age of these garnets, their ^{176}Hf/^{177}Hf show a much higher dispersity than other data and can therefore generate meaningful errorchrons. Thus, clinopyroxenes from spinel peridotite xenoliths from the northern part of the French Massif Central are much more amenable to Lu-Hf dating than those from many other regions of shallow sub-continental lithospheric mantle. Clinopyroxenes from mantle xenoliths from SW Poland may also be potential candidates for future Lu-Hf dating.

5. DISCUSSION

Extreme depletion in Hf and Zr in mantle xenoliths and their constituent clinopyroxenes from the northern part of the French Massif Central was earlier reported by Lenoir et al. (2000) and Downes et al. (2003). Our new LA-ICPMS analyses of clinopyroxenes confirm this anomaly and also confirm the presence of strong negative anomalies in Zr and Hf relative to the adjacent REE Sm and Nd in clinopyroxenes from mantle xenoliths from the Polish Sudetes (Figs. 2 and 3). Few other sub-continental mantle xenolith suites show this feature; those which do include some from southern Italy, western USA and southern Siberia. The extreme depletion in Hf and Zr is due to a process that removes these elements from the mantle, and the most obvious process is extensive partial melting. Wittig et al. (2006) modeled Hf depletion in clinopyroxenes in Massif Central peridotites as being due to extensive partial melting (e.g. up to 30%) in the spinel peridotite stability field. As shown in Figures 2-4, similar extreme Hf depletion of mantle clinopyroxenes has been reported for a mantle xenoliths from Avacha volcano, Kamchatka (Halama et al 2009).

One possible origin of this extensive mantle depletion may be related to supra-subduction zone processes. Since the volcanic fields of the northern Massif Central and the Polish Sudetes are all situated on the northern margin of the Variscan orogen, it is possible that the mantle beneath these regions experienced a similar extreme depletion event, which may require two-stage melting such as is found in the mantle wedge above a subducting slab. The Hf-depleted mantle clinopyroxene from Avacha volcano comes from a subduction setting (Halama et al., 2009). Tok (SE Siberia) and the Bearpaw Mountains (Montana) are in cratonic settings but are situated above regions of recent deep subduction, which may have been the cause of extreme depletion due to partial melting. Both Monte Vulture and Sicily are near to subduction zones, and the mantle beneath these regions may also have experienced strong depletion in this tectonic setting. However, the reason why such extensive melting has only occurred in some parts of the continental lithosphere is not entirely clear.

Comparison of the highly incompatible trace elements in mantle peridotite clinopyroxenes from the northern Massif Central and SW Poland (Figures 2 and 3) suggests that the lithospheric mantle beneath the two regions experienced different enrichment processes. In the northern Massif Central, clinopyroxenes show relative enrichment in U, La, Pb and Sr, compared to adjacent elements in their mantle-normalised patterns. Mantle-normalised Nb concentrations (Nb_n) are usually lower than Ta_n values; mantle-normalised Zr_n values are less than Hf_n values. In contrast, the Polish mantle peridotite xenoliths have clinopyroxenes that are relatively enriched in Nb (Fig. 3), with mantle-normalised Nb_n always greater than Ta_n, and with many showing enrichment in Zr relative to Hf. Unusually, Pb shows a relative depletion compared with the adjacent REE.

The contrasting trace element signatures of Zr-Hf depleted clinopyroxenes in the xenoliths from France and Poland are probably derived from contrasting metasomatic fluids. Among the northern Massif Central xenoliths, the enrichment in fluid-mobile elements such as U, Pb and Sr, and lack of enrichment in fluid-immobile ones, suggests that a subduction-related fluid may have been responsible. The lack of enrichment in Zr relative to Hf also implies that the fluid carried little or no Zr. Although both Lenoir et al. (2000) and Wittig et al. (2006) suggested that the metasomatic agent in these xenoliths might be a mantle-derived carbonatite magma, a subduction-related fluid, enriched in U, Pb, Sr and LREE, is also possible.

In contrast, the Polish xenoliths show enrichment in both LREE and the immobile elements (Zr, Nb), and additionally many of them have Zr_n greater than Hf_n, suggesting that the metasomatic agent carried some Zr. This may be the result of metasomatism by an alkaline silicate melt, which can carry such high-field strength elements. Again this is in contrast to the earlier suggestion (Blusztajn and Shimizu 1994) that carbonatite metasomatism had affected these samples. Zr-Hf depleted mantle clinopyroxenes from spinel peridotites from elsewhere in the world (Figure 4) tend to resemble those from Poland in terms of their enrichment in Zr relative to Hf, and the presence of Pb troughs, suggesting that they have also experienced silicate melt metasomatism to some extent.

Significantly, in the Polish xenoliths, the Zr_n values are less than Hf_n only in those samples which show lowest overall values of Zr_n and Hf_n, i.e. the most depleted samples (Fig. 3). In the less depleted samples, Zr_n is greater than Hf_n, indicating that Zr has been added to the clinopyroxenes after the original depletion had occurred. In contrast, in the northern Massif Central samples, Zr_n is generally less than Hf_n, for all samples, so there is no evidence of addition of Zr to the clinopyroxenes after the initial loss of both Zr and Hf by partial melting.

Figure 5 shows that only a few mantle peridotites worldwide display a trend towards high Lu/Hf ratios and low Hf contents in their clinopyroxenes. Other xenoliths have clinopyroxene compositions that cluster around Lu/Hf ratios between 0.1 and 1.0, and some suites show very little dispersion of Lu/Hf ratios. The trend shown by the clinopyroxene trace element data on Figure 5 is almost certainly due to removal of Hf relative to Lu, during partial melting of the mantle, since Hf is more incompatible than Lu in the shallow mantle. Another possible reason for Lu-Hf fractionation may be the earlier presence of garnet in the region of the mantle now represented by the spinel peridotite xenoliths (i.e. garnet became unstable because of a decrease in pressure perhaps by rifting or mantle uplift). Evidence for this may be present as vermicular spinel-pyroxene clusters described in Northern Massif Central xenoliths by Lenoir et al (2000) and Downes et al. (2003), which are commonly considered to be relics of pre-existing garnet.

Over geological time these high Lu/Hf ratios will lead to extremely radiogenic εHf values. In the example of the northern French Massif Central (Fig. 6), such xenoliths show highly radiogenic Hf isotope ratios (εHf values up to +2600). Thus, as shown in Fig. 7, in the northern Massif Central εHf values in clinopyroxenes from mantle peridotite xenoliths are much more strongly decoupled from εNd values compared with, for example, xenoliths from the oceanic lithosphere (e.g., Hawaii) or other regions of the sub-continental lithospheric mantle (e.g. the Lherz massif in the French Pyrenees; Le Roux et al., 2009). They appear to be extreme examples of spinel peridotite mantle with highly radiogenic Hf isotopes. Only rare xenoliths from Jordan and one from Hawaii show εHf values greater than 100, although unpublished data for mantle samples from Beni Bousera and Kaapvaal appear to have similarly extreme values (Pearson et al., 2003).

Clinopyroxenes with high Lu/Hf ratios from the northern Massif Central (Wittig et al., 2006) yield Hf model ages and $^{176}Hf/^{177}Hf$-$^{176}Lu/^{177}Hf$ systematics that appear to indicate that an event occurred in the mantle beneath this region in Variscan times (Fig. 8). A fundamental problem with dating mantle samples is to know what exactly is being dated. It is not clear whether the apparent Variscan age given by the Lu-Hf systematics of Massif Central mantle clinopyroxenes actually dates a specific event (e.g. depletion of Hf relative to Lu due to extensive melting). It might instead date the time at which the mantle passed through the closure temperature of Lu-Hf in clinopyroxene, although this temperature is not well constrained.

Other attempts at using Lu-Hf isotopes to date mantle events (e.g. Schmidberger et al., 2002; Choi et al., 2010) have been based on much smaller variations in $^{176}Hf/^{177}Hf$-$^{176}Lu/^{177}Hf$ ratios (Fig. 8) that are unlikely to yield meaningful results unless the event being dated is very old. One possible approach may be to use orthopyroxene mineral separates as well as clinopyroxene as, although orthopyroxene generally contains much less Hf than clinopyroxene (by an order of magnitude according to Dobosi et al (2010)), the modal abundance of orthopyroxene in spinel peridotites is often 2-3 times that of clinopyroxene, so a significant fraction of the Hf in the rock will reside within the orthopyroxene component. Mantle orthopyroxenes often show positive Zr and Hf anomalies compared to adjacent elements; indeed, orthopyroxene from northern Massif Central samples Mb8 and Mb57 show positive Hf anomalies, but the Hf abundance in the orthopyroxene is an order of magnitude less than that in the coexisting clinopyroxene (J. Puziewicz and M. Matusiak-Malek, pers. comm. 2013). Data presented by Dobosi et al. (2010) show that the Lu/Hf ratio in mantle peridotite orthopyroxene usually exceeds that of coexisting clinopyroxene by a factor of ~2. Thus it may be possible to use orthopyroxene to extend the Lu-Hf isochron, although analyzing the low levels of Hf in orthopyroxene may present technical problems.

6. CONCLUSIONS

The use of the Lu-Hf system for dating events in the shallow (spinel peridotite) lithospheric mantle is constrained by the behaviour of Lu and Hf during melting and metasomatism. Lu concentrations in mantle clinopyroxenes tend not to vary greatly, whereas Hf concentrations show wider variations as a result of depletion by partial melting. Thus the variation in Lu/Hf within mantle clinopyroxenes will govern the usefulness of the system to geochronology. Only a few rare peridotites show appropriate depletion in Hf compared with Lu in their clinopyroxenes. Among these, the example from the xenoliths from the northern part of the French Massif Central yields a geologically meaningful age of 350 Ma, attributed to depletion during Variscan subduction. These samples have not experienced addition of Hf during subsequent metasomatism, probably because the subduction-related metasomatic fluids that affected them carried little Hf. Other regions of central Europe, e.g. Lower Silesia (Poland) and the Bohemian Massif (Czech Republic), have mantle xenoliths which show Hf-depletion, but they have experienced later addition of Zr (and therefore perhaps Hf) during metasomatism and therefore may be less likely to produce meaningful Lu-Hf model ages or errorchrons.

Acknowledgements

We thank Andy Beard, Andy Carter and Martin Rittner (all at Birkbeck) for help with the ICP-MS analyses, Jacek Puziewicz and Magda Matusiak-Malek (Wroclaw, Poland) for additional LA-ICPMS determinations, and Jerzy Blusztajn (WHOI) for providing the samples from Poland. We appreciate the constructive comments on this manuscript from Elis Hoffmann, Ralf Halama, Sonja Aulbach, Sebastian Tappe, Theo Ntaflos, Dimitri Ionov and Laurie Reisberg.

References

Ackerman L, Medaris G, Spacek P and Ulrych J 2014. Geochemical and petrological constraints on mantle composition of the Ohre (Eger) rift, Bohemian Massif: peridotite xenoliths from the Ceske Stredohori volcanic complex and northern Bohemia. Int. J. Earth Sci. in press.

Arai S and Ishimaru S 2008. Insights into petrological characteristics of the lithosphere of mantle wedge beneath arcs through peridotite xenoliths: a review. J Petrol. 49, 665-695.

Aulbach S, Griffin W L, O’Reilly S Y and McCandless T E 2004. Genesis and evolution of the lithospheric mantle beneath the Buffalo Head Terrane, Alberta (Canada). Lithos 77, 413-451.

Babuska V, Plomerova J and Vecsey L., 2002. Seismic anisotropy of the French Massif Central and predisposition of Cenozoic rifting and volcanism by Variscan suture hidden in the mantle lithosphere. Tectonics 21, 1-20.

Bianchini G, Beccaluva L, Bonadiman C, Nowell G, Pearson G, Siena F and Wilson M 2007. Evidence of diverse depletion and metasomatic events in harzburgite-lherzolite mantle xenoliths from the Iberian plate (Olot, NE Spain): implications for lithosphere accretionary processes. Lithos 94, 25-45.

Bizimis M, Griselin M, Lassiter J C, Salters V J M and Sen G 2007. Ancient recycled mantle lithosphere in the Hawaiian plume: Osmium-Hafnium isotopic evidence from peridotite mantle xenoliths. Earth Planet Sci. Lett. 257, 259-273.

Blusztajn J and Shimizu N, 1994.The trace element variations in clinopyroxenes from spinel peridotite xenoliths from southwest Poland. Chem. Geol. 111, 227-243.

Bonadiman C, Coltorti M, Duggen S, Paludetti L, Siena F, Thirlwall M F and Upton B G J 2008. Palaeozoic subduction related and kimberlite or carbonatite metasomatism in the Scottish lithospheric mantle. In: Coltorti M and Gregoire M (eds). *Metasomatism in Oceanic and Continental Lithospheric Mantle.* Geol. Soc. Lond. Sp. Pub. 293, 303-333.

Choi S H, Suzuki K, Mukasa S B, Lee J-I and Jung H, 2010. Lu-Hf and Re-Os systematics of peridotite xenoliths from Spitsbergen, western Svalbard: implications for mantle-crust coupling. Earth Planet. Sci. Lett. 297, 121-132.

Deng, F.L. and McDougall, J.D., 1992. Proterozoic depletion of the lithosphere recorded in mantle xenoliths from Inner Mongolia. Nature, 360: 333-336.

Dobosi G, Jenner G A, Embey-Isztin A and Downes H 2010. Cryptic metasomatism in clino- and orthopyroxene in the upper mantle beneath the Pannonian region. In: *Petrological Evolution of the European Lithospheric Mantle.* Geol. Soc. London. Sp. Pub. 337, 177-194.

Downes H, Kostoula T, Jones A, Beard A, Thirlwall M and Bodinier J-L 2002. Geochemistry and Sr-Nd isotopic compositions of mantle xenoliths from the Monte Vulture carbonatite-melilitite volcano, central southern Italy. Contrib. Mineral. Petrol. 144, 78-92.

Downes H, Reichow M K, Mason P R D, Beard A D and Thirlwall M F 2003. Mantle domains in the lithosphere beneath the French Massif Central: trace element and isotopic evidence from mantle clinopyroxenes. Chemical Geology 200, 71-87.

Downes, H., Macdonald, R., Upton, B.G.J., Cox, K.G., Bodinier, J-L., Mason, P.R.D., James, D., Hill, P.G. and Hearn.B.C. Jr. 2004. Ultramafic xenoliths from the Bearpaw Mountains, Montana, USA: Evidence for multiple metasomatic events in the lithospheric mantle beneath the Wyoming Craton. Journal of Petrology 45, 1631-1662.

Femenias O, Coussaert N, Bingen B, Whitehouse M, Mercier J-C C and Demaiffe D 2003. A Permian underplating event in late- to post-orogenic tectonic setting. Evidence from the mafic-ultramafic layered xenoliths from Beaunit (French Massif Central). Chem. Geol. 199, 293-315.

Gonzaga R G, Menzies M A, Thirlwall M F, Jacob D E and LeRoex A 2010. Eclogites and garnet pyroxenites: Problems resolving provenance using Lu-Hf, Sm-Nd and Rb-Sr isotope systems. J. Petrology 51, 513-535.

Gregoire M, Tinguely C, Bell D R and le Roex A P 2005. Spinel lherzolite xenoliths from the Premier kimberlite (Kaapvaal craton, South Africa): Nature and evolution of the shallow upper mantle beneath the Bushveld complex. Lithos 84, 185-205.

Halama R, Savov I P, Rudnick R L, McDonough W F 2009. Insights into Li and Li isotope cycling and sub-arc metasomatism from veined mantle xenoliths, Kamchatka. Contrib. Mineral. Petrol. 158, 197-222.

Handler, M.R., Wysoczanski, R.J. and Gamble, J.A., 2003. Proterozoic lithosphere in Marie Byrd Land, West Antarctica: Re-Os systematics of spinel peridotite xenoliths. Chemical Geology, 196: 131-145.

Ionov D A 2004. Chemical variations in peridotite xenoliths from Vitim, Siberia: Inferences for REE and Hf-behaviour in the garnet-facies upper mantle. J Petrol. 45, 343-367.

Ionov D A, Chazot G, Chauvel C, Merlet C, Bodinier J L 2006a. Trace element distribution in peridotite xenoliths from Tok, SE Siberian craton: A record of pervasive multi-stage metasomatism in the shallow refractory mantle. Geochim. Cosmochim. Acta 70, 1231-1260.

Ionov D A, Shirey S B, Weiss D and Brugmann G 2006b. Os-Hf-Sr-Nd isotope and PGE systematics of spinel peridotite xenoliths from Tok, SE Siberian craton: Effects of pervasive metasomatism in the shallow refractory mantle. Earth Planet. Sci. Lett. 241, 47-64.

Ishimaru S, Arai S, Ishida Y, Shirasaka M, and Okrugin M, 2007. Meltiung and multi-stage metasomatism in the mantle wedge beneath a frontal arc inferred from highly depleted peridotites xenoliths from the Avacha volcano, southern Kamchatka. J. Petrol. 48, 395-433.

Janney P E, Shirey S B, Carlson R W, Pearson D G, Bell D R, Le Roex A P, Ishikawa A, Nixon P H and Boyd F R 2010. Age, composition and thermal characteristics of South African off-craton mantle lithosphere: evidence for a multi-stage history. J. petrology, 51, 1849-1890.

Lazarov M, Brey G P and Weyer S 2009. Time steps of depletion and enrichment in the Kaapvaal craton as recorded by subcalcic garnets from Finsch (SA). Earth Planet. Sci. lett 279, 1-10.

Lenoir X, Garrido C J, Bodinier J and Dautria J 2000. Contrasting lithospheric mantle domains beneath the Massif Central (France) revealed by geochemistry of peridotite xenoliths. Earth Planet. Sci. Lett. 181, 359-375.

Le Roux V, Bodinier J-L, Alard O, S Y and Griffin W L 2009. Isotopic decoupling of Hf, Nd and Sr during porous melt flow: a case study in the Lherz peridotites (Pyrenees). Earth Planet. Sci. Lett. 279, 76-85.

Marks M, Halama R, Wenzel T and Markl G 2004. Trace element variations in clinopyroxene and amphibole from alkaline to peralkaline syenites and granites: implications for mineral-melt trace-element partitioning. Chem. Geol. 211, 185-215.

Mason P, Jarvis K E, Downes H and Vannucci R 1999. Determinations of incompatible trace elements in mantle clinopyroxenes by LA-ICP-MS: a comparison of analytical performance with established techniques. J of Geostand. Geoanalysis, 23, 157-172.

Matusiak-Malek, M., Puziewicz, J., Ntaflos, T., Grégoire, M. & Downes, H. 2010. Metasomatic effects in the lithospheric mantle beneath the NE Bohemian Massif: A case study of Lutynia (SW Poland) peridotite xenoliths. Lithos 117, 49-60.

McInnes B I A, Gregoire M, Binns R A, Herzig P M and Hannington M D, 2001. Hydrous metasomatism of oceanic sub-arc mantle, Lihir, Papua New Guinea: petrology and geochemistry of fluid-metasomatised mantle wedge xenoliths. Earth Planet. Sci. Lett. 188, 169-183.

Nasir S and Rollinson H 2009. The nature of the subcontinental lithospheric mantle beneath the Arabian Shield: Mantle xenoliths from southern Syria. Precambrian Research 172, 323-333.

Pearson D G, Canil D and Shirey S B 2003. Mantle samples included in volcanic rocks: Xenoliths and diamonds. Treatise on Geochemistry vol 2, Section 2.05.

Pearce N J G, Perkins W T, Westgate J A, Gorton M P, Jackson S E, Neal C R and Chenery S P 1997. A compilation of new and published major and trace element data for NIST SRM 610 and NIST SRM 612 glass reference standards. Geostand. Newsletter 21, 115-144.

Perinelli C, Sapienza G T, Armienti P and Morten L 2008. Metasomatism of the upper mantle beneath the Hyblean Plateau (Sicily): evidence from pyroxenes and glass in peridotite xenoliths. In: Coltorti M and Gregoire M (eds). *Metasomatism in Oceanic and Continental Lithospheric Mantle.* Geol. Soc. Lond. Sp. Pub. 293, 197-221.

Puziewicz, J., Koepke, J., Grégoire, M., Ntaflos, T. & Matusiak-Malek, M. 2011. Lithospheric Mantle Modification during Cenozoic Rifting in Central Europe: Evidence from the Ksieginki Nephelinite (SW Poland) Xenolith Suite. Journal of Petrology 52, 2107-2145.

Rampone E and Hofmann A W 2012. A global overview of isotopic heterogeneities in the oceanic mantle. Lithos 148, 247-261.

Rudnick, R.L. and Walker, R.J., 2009. Interpreting ages from Re–Os isotopes in peridotites. Lithos 112 (S), 1083-1095.

Sanchez-Rodriguez L and Gebauer D 2000. Mesozoic formation of pyroxenites and gabbros in the Ronda area (southern Spain), followed by early Miocene subduction metamorphism and emplacement into the middle crust: U-Pb sensitive high-resolution ion microprobe dating of zircon. Tectonophysics 316, 19-44.

Scherer E, Münker C and Mezger K., 2001. Calibration of the Lutetium-Hafnium Clock. Science 293, 683-687.

Schmidberger S S, Simonetti A and Francis D 2001. Sr-Nd-Pb isotope systematics of mantle xenoliths from Somerset Island kimberlites: Evidence for lithosphere stratification beneath Arctic Canada. Geochim. Cosmochim. Acta. 65, 4243-4255.

Schmidberger S S, Simonetti A, Francis D and Gariepy C 2002. Probing Archean lithosphere using the Lu-Hf isotope systematics of peridotite xenoliths from Somerset Island kimberlites, Canada. Earth Planet. Sci. Lett. 197, 245-259.

Schmidberger S S, Simonetti A, Heaman L M, Creaser R A and Whiteford S 2007. Lu-Hf, in-situ Sr and Pb isotope and trace element systematics for mantle eclogites from the Diavik diamond mine: Evidence for Palaeoproterozoic subduction beneath the Slave craton, Canada. Earth Planet. Sci. Lett. 254, 55-68.

Schmidt, G. and Snow, J., 2002. Os isotopes in mantle xenoliths from the Eifel volcanic field and the Vogelsberg (Germany): age constraints on the lithospheric mantle. Contributions to Mineralogy and Petrology, 143: 694-705.

Shaw J E, Baker J A, Kent A J R, Ibrahim K M and Menzies M A, 2007. The geochemistry of the Arabian lithospheric mantle – a source for intraplate volcanism? J. Petrol. 48, 1495-1512.

Shu Q, Brey G P, Gerdes A and Hofer H 2013. Geochronological and geochemical constraints on the formation and evolution of the mantle underneath the Kaapvaal craton: Lu-Hf and Sm-Nd systematics of subcalcic garnets from highly depleted peridotites. Geochimica et Cosmochimica Acta 113, 1-20.

Söderlund U, Patchett P J, Vervoort J D and Isachsen C E 2004. The ^{176}Lu decay constant determined by Lu-Hf and U-Pb isotope systematics of Precambrian mafic intrusions. Earth Planet. Sci. Lett.

Stracke A, Snow J E, Hellebrand E, von der Handt A, Bourdon B, Birbaum K and Günther D, 2011. Abyssal peridotites Hf isotopes identify extreme mantle depletion. Earth Planet. Sci. Lett. 308, 359-368.

Sun S-S and McDonough W F 1989. Chemical and isotopic systematics of ocean basalts: implications for mantle composition and processes. In: Saunders A D and Norry M J (Eds). Magmatism in the Ocean Basins. Geol. Soc. Sp. Pub. 42, 313-345.

Tappe S, Smart K A, Pearson D G, Steenfelt A and Simonetti A 2011. Craton formation in Late Archean subduction zones revealed by first Greenland eclogites. Geology, 39, 1103-1106.

Teklay M, Scherer E, Mezger K and Danyushevsky L 2010. Geochemical characteristics and Sr-Nd-Hf isotope compositions of mantle xenoliths and host basalts from Assab, Eritrea: implications for the composition and thermal structure of the lithosphere beneath the Afar Depression. Contrib. Mineral. Petrol. 159, 731-351.

Vannucci R, Ottolini L, Bottazzi P, Downes H and Dupuy C 1994. INAA, IDMS and SIMS comparative REE investigations of clinopyroxenes from mantle xenoliths with different textures. Chem. Geol. 118. 85-108.

Widom, E., Kepezhinskas, P. and Defant, M., 2003. The nature of metasomatism in the sub-arc mantle wedge: evidence from Re-Os isotopes in Kamchatka peridotite xenoliths. Chemical Geology, 196: 283-306.

Witt-Eickschen G and Kramm U 1997. Mantle upwelling and metasomatism beneath central Europe: Geochemical and isotopic constraints from mantle xenoliths from the Rhön (Germany). J. Pet. 38, 479-493.

Wittig N, Baker J A, Downes H 2006. Dating the mantle roots of young continental crust. Geology 34, 237-240.

Wittig N, Baker J A, Downes H 2007. U-Th-Pb and Lu-Hf isotopic constraints on the evolution of sub-continental lithospheric mantle, French Massif Central. Geochim. Cosmochim. Acta, 71, 1290-1311.

Wittig N, Pearson D G, Downes H and Baker J A 2009. The U, Th and Pb elemental and isotopic compositions of mantle clinopyroxenes and their grain boundary contamination derived from leaching and digestion experiments. Geochim. Cosmochim. Acta, 73, 469-488.

Wittig, N., Pearson, D.G., Baker, J.A., Duggen, S. and Hoernle, K., 2010a. A major element, PGE and Re-Os isotope study of Middle Atlas (Morocco) peridotite xenoliths: Evidence for coupled introduction of metasomatic sulphides and clinopyroxene. Lithos, 115: 15-26.

Wittig, N. Webb M, Pearson D G, Dale C W, Ottley C J, Hutchison M, Jensen S M and Luget A., 2010b. Formation of the North Atlantic Craton: Timing and mechanisms constrained from Re-Os isotope and PGE data of peridotite xenoliths from S.W. Greenland. Chemical Geology, 276: 166-187.

Wittig N, Pearson D G, Duggen S, Baker J A and Hoernle K, 2010c. Tracing the metasomatic and magmatic evolution of continental mantle roots with Sr, Nd, Hf and Pb isotopes: a case study of Middle Atlas (Morocco) peridotite xenoliths. Geochim. Cosmochim. Acta. 74, 1417-1435.

Xu X, Griffin W L, O'Reilly S Y, Pearson N J, Geng H and Zheng J, 2008. Re-Os isotopes of sulfides in mantle xenoliths from eastern China: progressive modification of the lithospheric mantle. Lithos 102, 43-64.

Yu J-H, O'Reilly S Y, Zhang M, Griffin W L and Xu X 2006. Roles of melting and metasomatism in the formation of the lithospheric mantle beneath the Leizhou peninsula, south China. J. Pet. 47, 355-383.

Yu S-Y, Xu Y-G, Huang X-L, Ma J-L, Ge W-C, Zhang H-H and Qin X-F 2009. Hf-Nd isotopic decoupling in continental mantle lithosphere beneath Northeast China: effects of pervasive mantle metasomatism. J. Asian Earth Sci. 35, 554-570.

Zangana N A 1995. Geochemical variations in mantle xenoliths from Ray pic, Massif Central, france. Unpub. PhD thesis, University of London.

Zangana NA, Downes H, Thirlwall M F, Marriner G F and Bea F 1998. Geochemical variation in peridotite xenoliths and their constituent clinopyroxenes from Ray Pic

(French Massif Central): implications for the composition of the shallow lithospheric mantle. Chem. Geol. 153, 11-35.

Zheng J, Griffin W L, O'Reilly S Y, Zhang M and Pearson N, 2006. Zircons in mantle xenoliths record the Triassic Yangtze-North China continental collision. Earth Planet. Sci. Lett. 247, 130-142.

Figure Captions

Figure 1 Sm/Nd vs Lu/Hf ratios in clinopyroxenes from spinel peridotite mantle rocks from worldwide localities. Data Sources: NFMC = North French Massif Central (Table 1); SFMC = South French Massif Central (Table1); Poland (Table 2); Pannonian Basin (unpublished data, CDV); Jordan (Shaw et al., 2007); China (Leizhou –Yu et al., 2006); Vulture (Italy - Downes et al., 2002); Rhön (Witt-Eickschen and Kramm, 1997); Tok, Siberia (Ionov et al., 2006); Hawaii (Bizimis et al., 2007); Premier, South Africa (Gregoire et al., 2005); Bearpaws, Montana, USA (Downes et al., 2004); Morocco (Wittig et al., 2010c); NE Spain (Bianchini et al., 2007); Alberta (Aulbach et al., 2004). Values for primitive mantle (Sm/Nd = 0.328; Lu/Hf = 0.239) from Sun and McDonough (1989).

Figure 2. LA-ICPMS data for clinopyroxene in representative mantle xenoliths from the Northern Massif Central compared with those of the Southern Massif Central (data from Table 1), normalised to primitive mantle (Sun and McDonough 1989). Data shown by grey squares and dashed line are for clinopyroxene in mantle xenoliths from Avacha volcano, Kamchatka, situated above an active subduction zone (Halama et al., 2009).

Figure 3. LA-ICPMS data for clinopyroxene in mantle xenoliths from Polish Sudetes (data from Table 2) normalised to primitive mantle (Sun and McDonough 1989). Data shown by grey squares and dashed line are for clinopyroxene in mantle xenoliths from Avacha volcano, Kamchatka, situated above an active subduction zone (Halama et al., 2009).

Figure 4. Zr-Hf-depleted clinopyroxenes from mantle xenoliths from Mte Vulture Italy - Downes et al., 2002; Sicily - Perinelli et al., 2008; Bearpaw Mts (Wyoming - Downes et al., 2004), Middle Atlas (Morocco - Wittig et al., 2010c), Tok (Siberia - Ionov et al., 2006), Plesny (Bohemian massif -Ackerman et al., in press), normalised to primitive mantle (Sun and McDonough 1989). Data shown by grey squares and dashed line are for clinopyroxene in mantle xenoliths from Avacha volcano, Kamchatka, situated above an active subduction zone (Halama et al., 2009).

Figure 5. Lu/Hf ratio vs Hf concentration (ppm) in clinopyroxenes from mantle spinel peridotite xenoliths worldwide. Data sources as for Fig. 1. Note logarithmic scales on both axes. A few show extreme Hf-depletion and consequent high Lu/Hf ratios similar to those of the Southern French Massif Central. Arrow indicates increasing extent of partial melting. Values for primitive mantle from Sun and McDonough (1989). Data

shown by grey squares and dashed line are for clinopyroxene in mantle xenoliths from Avacha volcano, Kamchatka, situated above an active subduction zone (Halama et al., 2009).

Figure 6. εHf-εNd isotope data for clinopyroxenes from mantle spinel peridotite xenoliths from French Massif Central showing differences between northern and southern regions (Wittig et al., 2007). Inset shows expanded field of southern Massif Central samples compared with the field for Mid-Ocean Ridge Basalts and Ocean Island Basalts (dashed line).

Figure 7. εHf-εNd isotope data for clinopyroxenes from mantle peridotites worldwide (data sources as follows: Jordan – Shaw et al., 2007; Alberta – Aulbach et al., 2004; Hawaii – Bizmis et al., 2007; Tok – Ionov et al., 2006b; Somerset Island (Canada) – Schmidberger et al., 2001, 2002; Scotland – Bonadiman et al., 2008; Olot (Spain) – Bianchini et al., 2007; Middle Atlas (Morocco) – Wittig et al., 2010c; Eritrea – Teklay et al., 2010; NE China – Yu et al., 2009; Spitsbergen – Choi et al.., 2010; Lherz massif – Le Roux et al., 2009; Gakkel Ridge – Stracke et al., 2011), compared with εHf-εNd isotope data from clinopyroxenes from the northern Massif Central peridotite xenoliths (Wittig et al., 2007). The most enriched compositions from the northern Massif Central shown on Figure 6 have been omitted.

Figure 8. Lu-Hf isochron diagram for clinopyroxenes from spinel peridotite mantle xenoliths from the northern Massif Central, showing a reference isochron of 344±11 Ma (Wittig et al., 2006), compared to data from other regions of sub-continental lithospheric mantle (Schmidberger et al., 2002; Le Roux et al., 2009; Choi et al., 2010). Inset shows the reference isochron of 350±61Ma for the northern Massif Central samples minus the two with the highest Lu/Hf ratios.

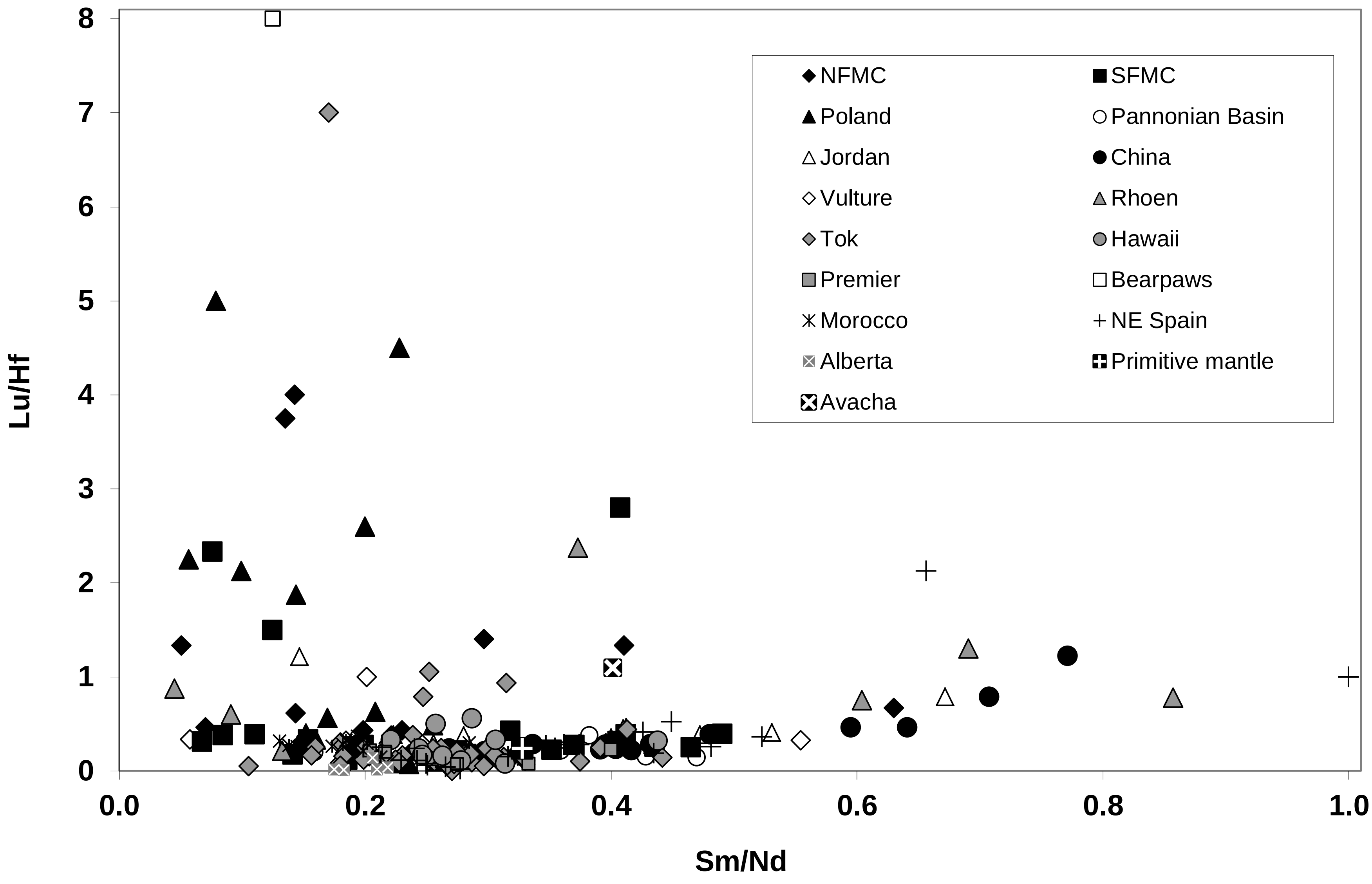
Lu/Hf
Sm/Nd
0
1
2
3
4
5
6
7
8
0.0
0.2
0.4
0.6
0.8
1.0
◆ NFMC
■ SFMC
▲ Poland
○ Pannonian Basin
△ Jordan
● China
◇ Vulture
▲ Rhoen
◆ Tok
● Hawaii
■ Premier
□ Bearpaws
⚹ Morocco
+ NE Spain
⊠ Alberta
⊞ Primitive mantle
⊠ Avacha

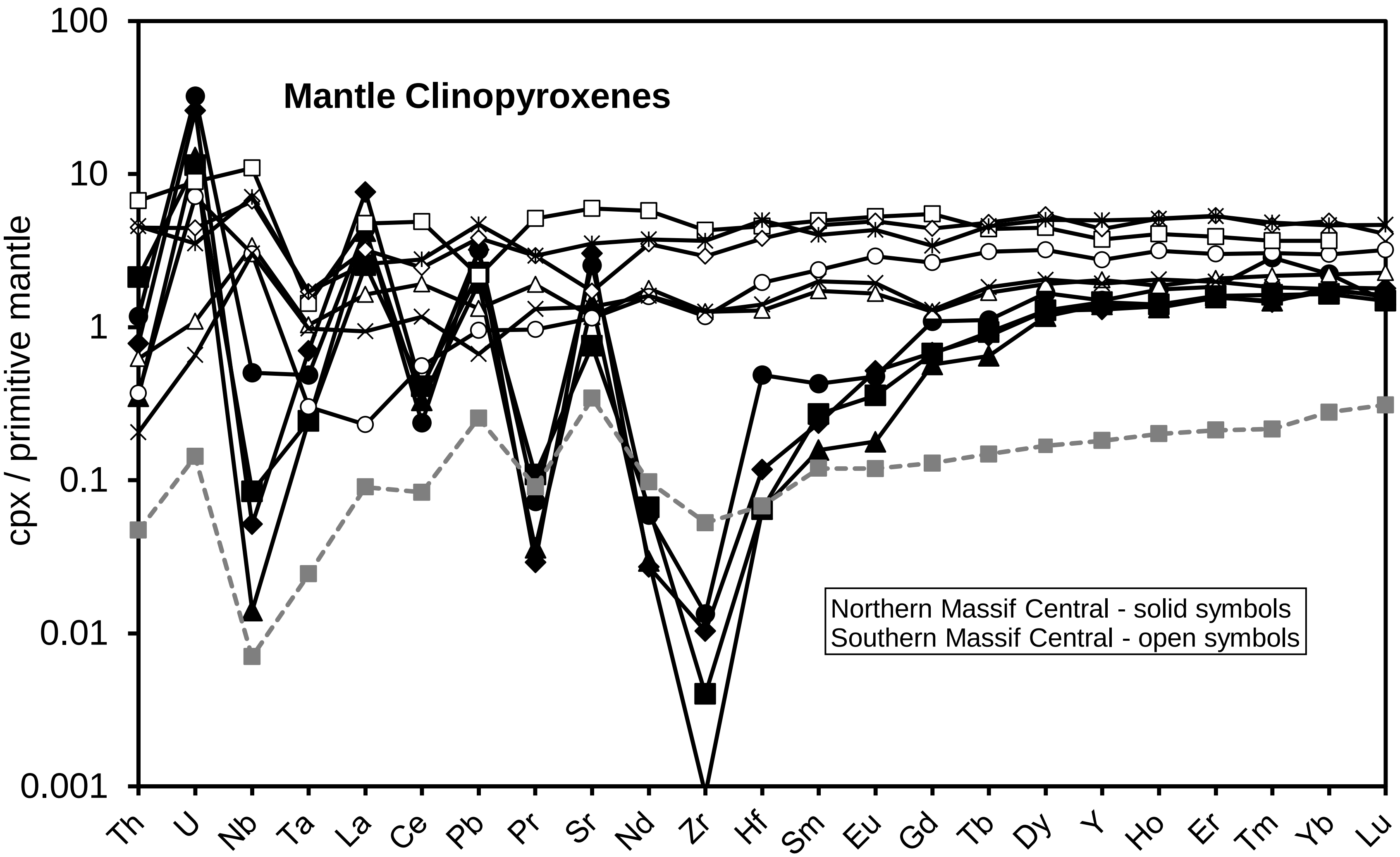
Mantle Clinopyroxenes
cpx / primitive mantle
100
10
1
0.1
0.01
0.001
Th
U
Nb
Ta
La
Ce
Pb
Pr
Sr
Nd
Zr
Hf
Sm
Eu
Gd
Tb
Dy
Y
Ho
Er
Tm
Yb
Lu
Northern Massif Central - solid symbols
Southern Massif Central - open symbols

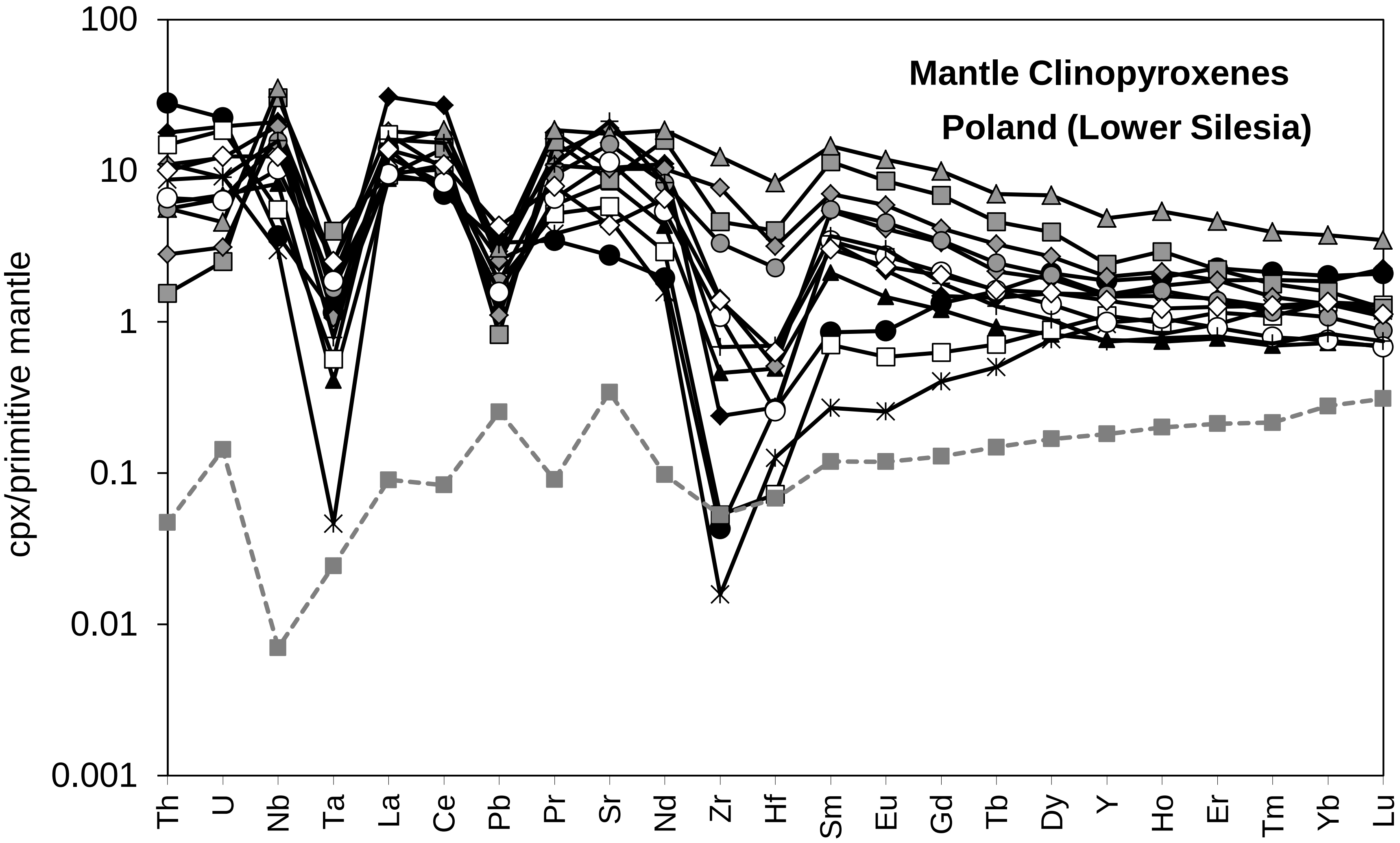
Mantle Clinopyroxenes
Poland (Lower Silesia)
cpx/primitive mantle
100
10
1
0.1
0.01
0.001
Th
U
Nb
Ta
La
Ce
Pb
Pr
Sr
Nd
Zr
Hf
Sm
Eu
Gd
Tb
Dy
Y
Ho
Er
Tm
Yb
Lu

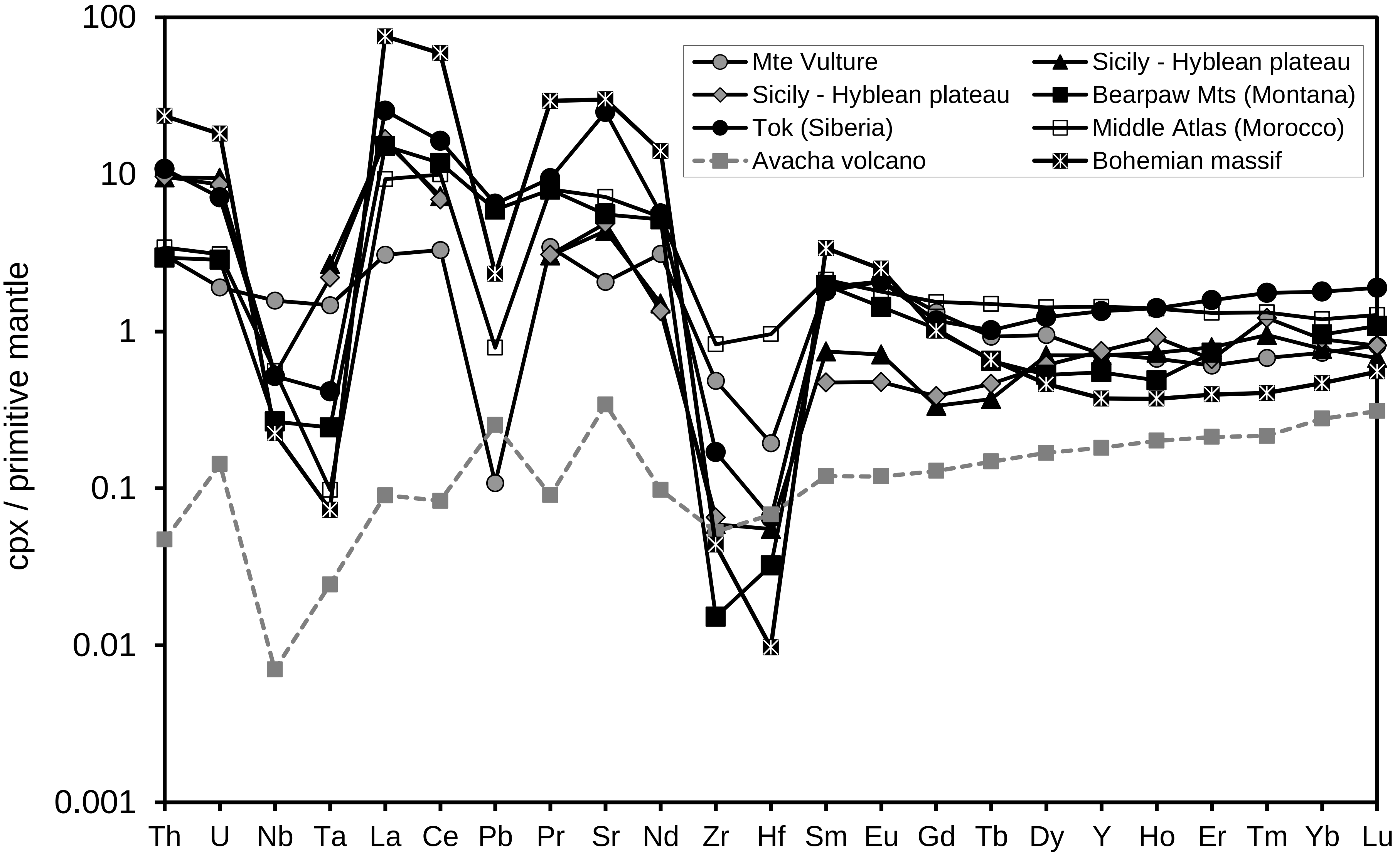
100
10
1
0.1
0.01
0.001
cpx / primitive mantle
Th
U
Nb
Ta
La
Ce
Pb
Pr
Sr
Nd
Zr
Hf
Sm
Eu
Gd
Tb
Dy
Y
Ho
Er
Tm
Yb
Lu
Mte Vulture
Sicily - Hyblean plateau
Tok (Siberia)
Avacha volcano
Sicily - Hyblean plateau
Bearpaw Mts (Montana)
Middle Atlas (Morocco)
Bohemian massif

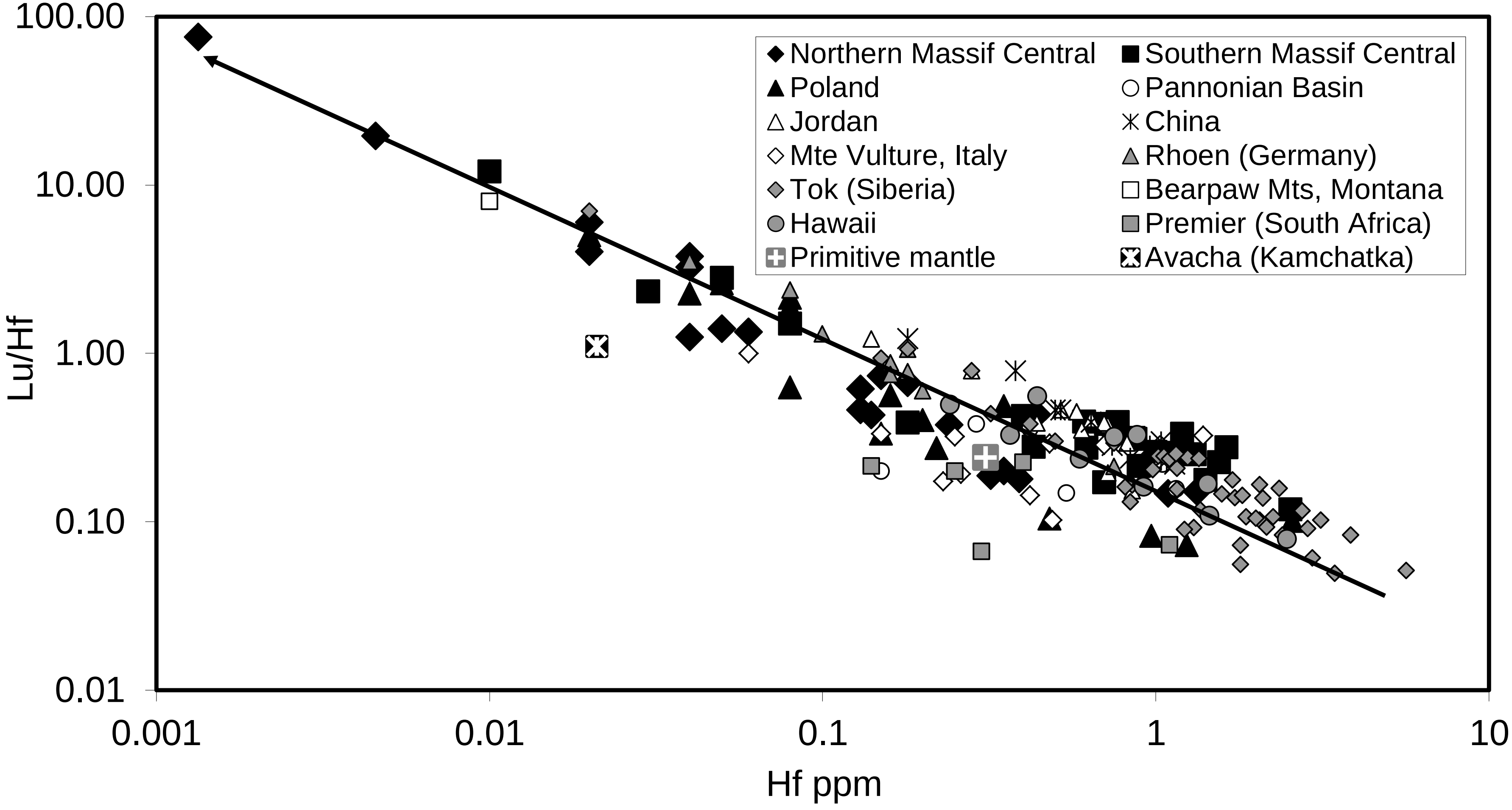
100.00
10.00
1.00
0.10
0.01
Lu/Hf
0.001
0.01
0.1
1
10
Hf ppm
◆ Northern Massif Central
■ Southern Massif Central
▲ Poland
○ Pannonian Basin
△ Jordan
✳ China
◇ Mte Vulture, Italy
▲ Rhoen (Germany)
◆ Tok (Siberia)
□ Bearpaw Mts, Montana
● Hawaii
■ Premier (South Africa)
✚ Primitive mantle
☒ Avacha (Kamchatka)

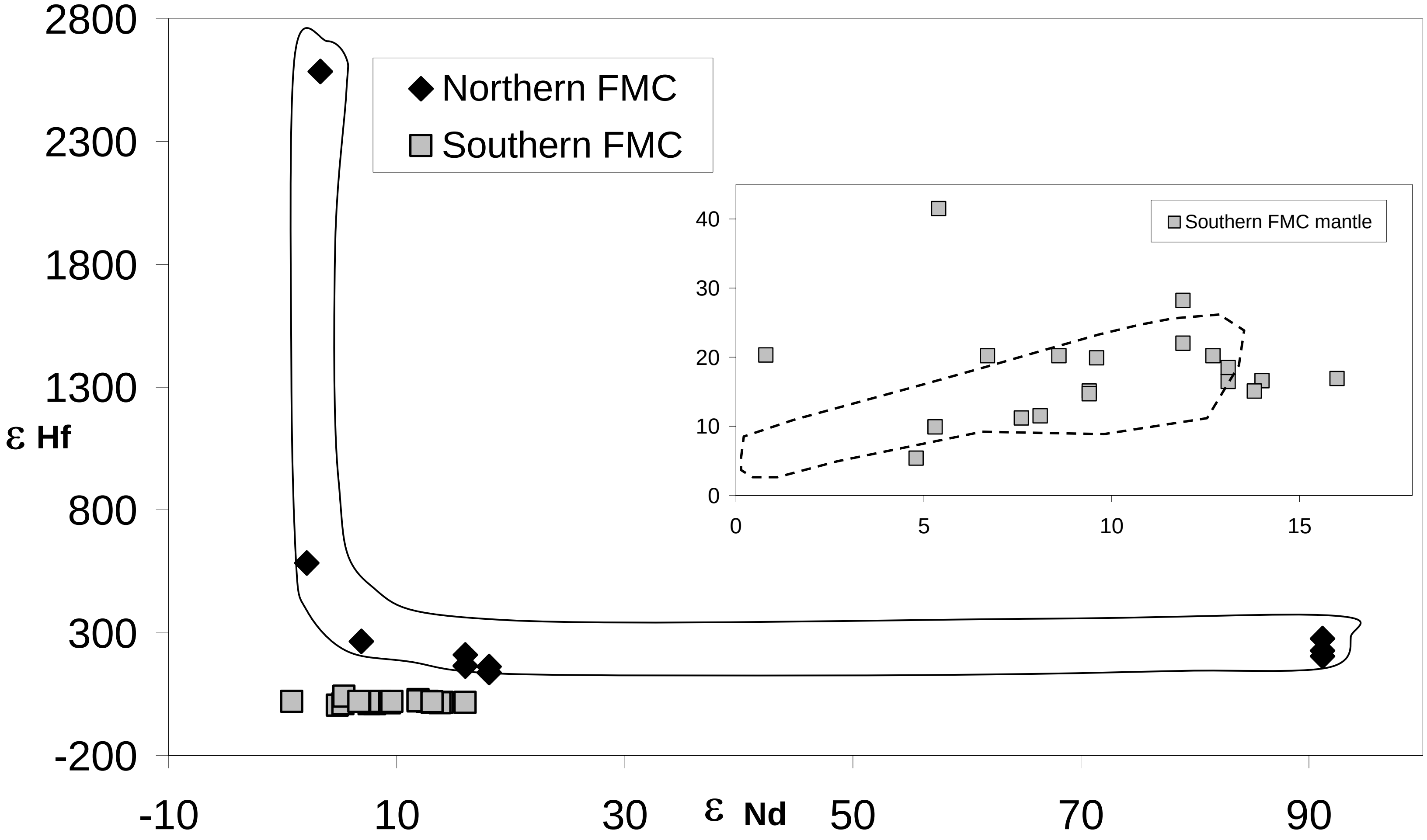
2800
2300
1800
1300
ε Hf
800
300
-200
-10
10
30
ε Nd
50
70
90
◆ Northern FMC
▨ Southern FMC
40
30
20
10
0
0
5
10
15
▨ Southern FMC mantle

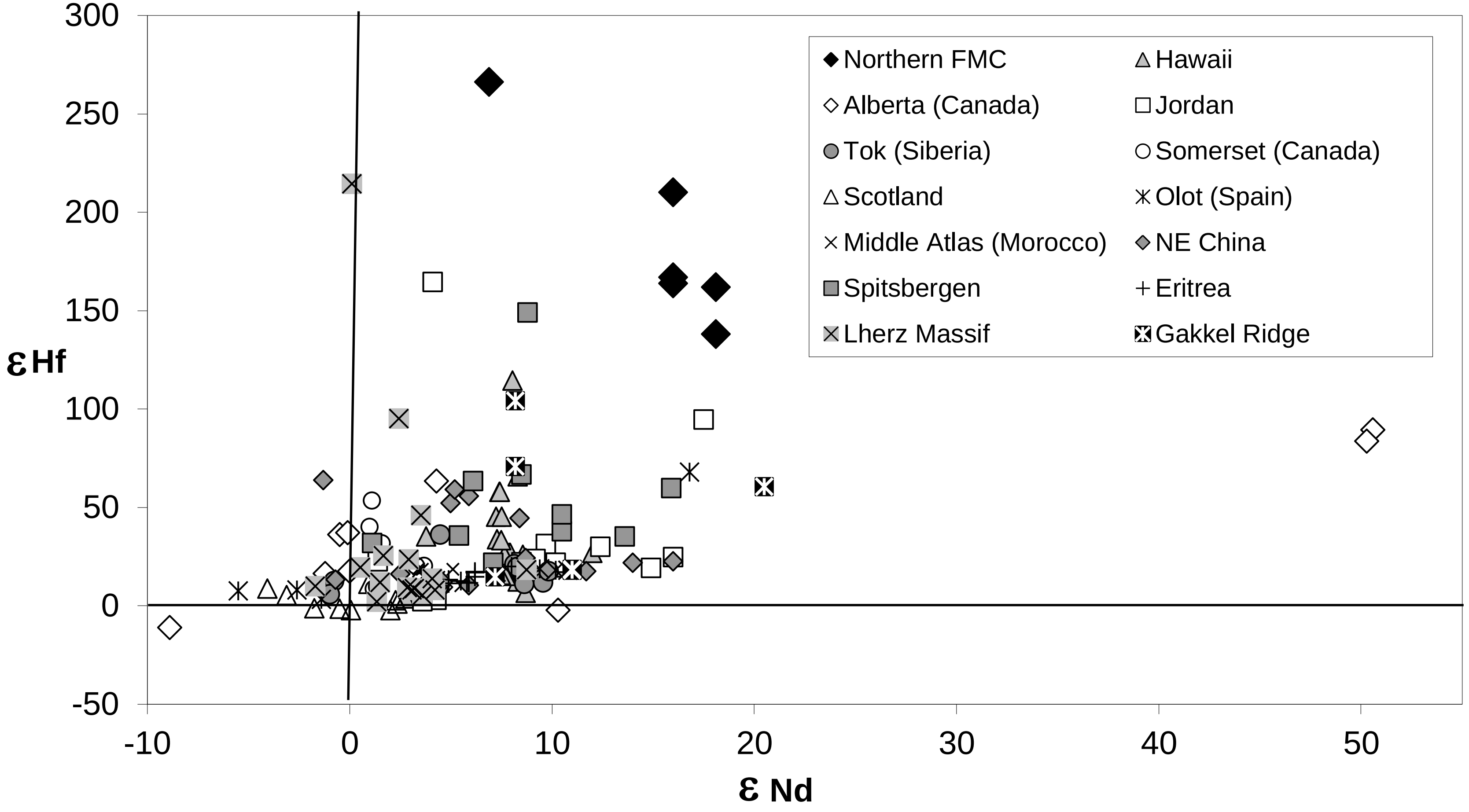
300
250
200
150
100
50
0
-50
ε Hf
-10
0
10
20
30
40
50
ε Nd
◆ Northern FMC
◇ Alberta (Canada)
● Tok (Siberia)
△ Scotland
× Middle Atlas (Morocco)
■ Spitsbergen
☒ Lherz Massif
▲ Hawaii
□ Jordan
○ Somerset (Canada)
⁎ Olot (Spain)
◆ NE China
+ Eritrea
☒ Gakkel Ridge

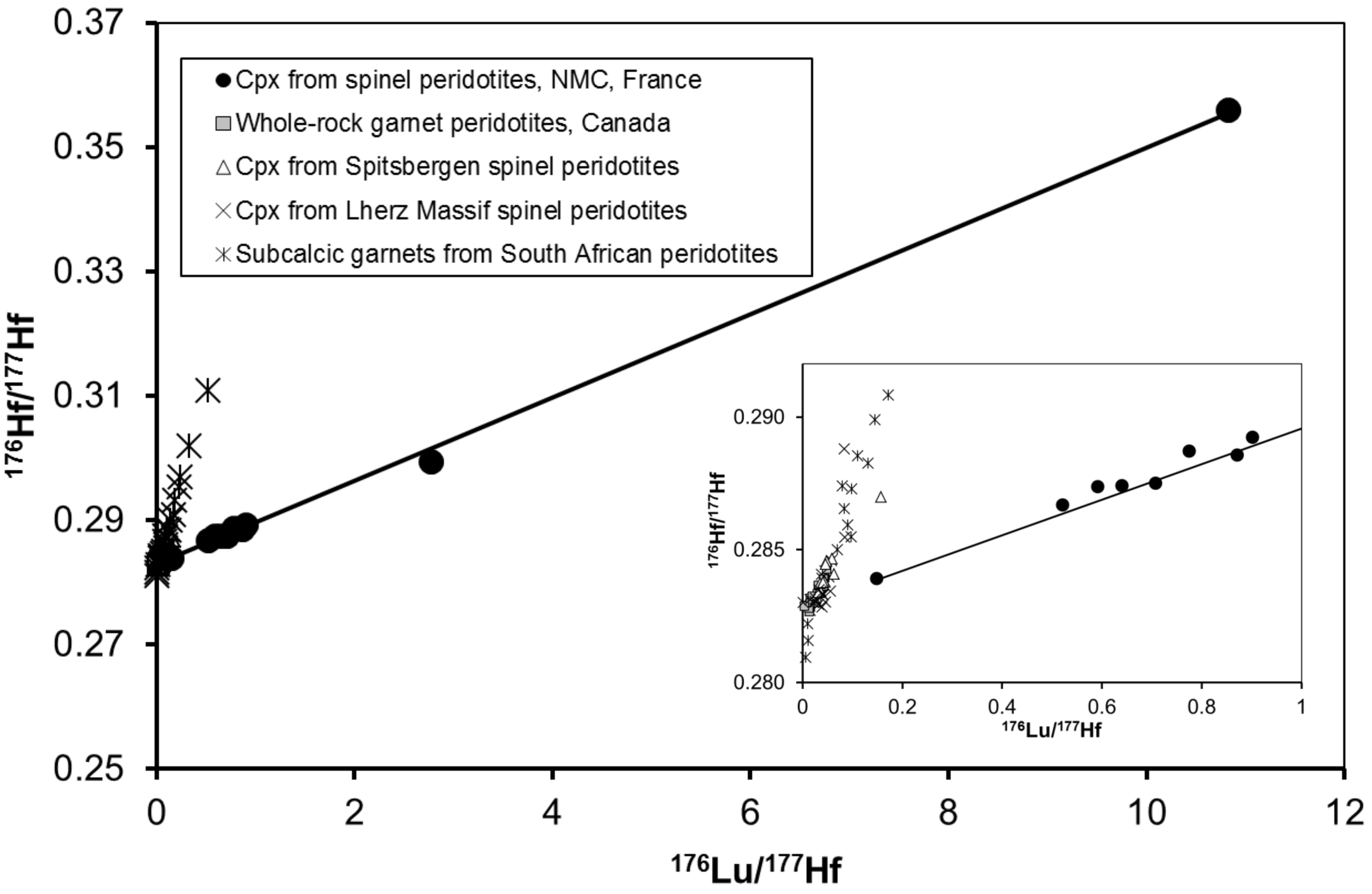
0.37
0.35
0.33
0.31
0.29
0.27
0.25
$^{176}Hf/^{177}Hf$
0
2
4
6
8
10
12
$^{176}Lu/^{177}Hf$
● Cpx from spinel peridotites, NMC, France
▨ Whole-rock garnet peridotites, Canada
△ Cpx from Spitsbergen spinel peridotites
× Cpx from Lherz Massif spinel peridotites
✳ Subcalcic garnets from South African peridotites
0.290
0.285
0.280
$^{176}Hf/^{177}Hf$
0
0.2
0.4
0.6
0.8
1
$^{176}Lu/^{177}Hf$

Table 1. Analyses of clinopyroxenes from French Massif Central, by LA-ICP-MS. NMC = Northern Domain

element	**RP83-72** **SMC**	**RP87-2** **SMC**	**RP91-20** **SMC**	**BO83-74** **SMC**	**Ta 7** **SMC**	**Ta 13** **SMC**	**Ta 19** **SMC**	**Gr83-75** **SMC**
Rb				0.01		0.03	0.02	0.02
Ba				0.05		0.31	0.27	0.09
Th	2.80	0.02	0.02	0.02	0.90	0.56	0.74	0.05
U	0.51	0.02	0.02	0.01	0.24	0.27	0.21	0.02
Nb	0.15	0.05	0.08	2.17	0.70	8.86	7.49	2.42
Ta	0.03	0.02	0.02	0.04	0.02	0.01	0.09	0.04
La	20.00	0.34	0.12	0.65	6.70	1.84	11.42	1.12
Ce	58.00	2.35	1.11	2.08	7.20	5.69	19.67	3.39
Pb	0.67	0.18	0.70	0.12	1.20	0.49	0.31	0.24
Pr	6.70	0.62	0.34	0.36	0.90	0.68	2.78	0.53
Sr	353.0	49.0	24.0	28.7	103.0	55.7	240.4	24.7
Nd	22.00	3.61	2.50	2.17	4.30	8.86	7.49	2.42
Zr	22.00	25.00	16.50	14.16	40.00	31.54	39.07	14.10
Hf	0.70	0.87	0.71	0.43	1.31	1.00	0.89	0.40
Sm	3.10	1.69	1.39	0.89	2.00	1.68	2.06	0.77
Eu	0.82	0.76	0.53	0.33	0.67	0.66	0.69	0.28
Gd	2.10	2.30	1.94	0.77	2.80	1.37	1.40	0.75
Tb	0.32	0.46	0.42	0.20	0.54	0.44	0.39	0.18
Dy	1.80	2.90	2.80	1.51	3.70	3.29	2.63	1.41
Y	10.00	19.30	18.40	8.78	23.00	29.94	11.87	9.25
Ho	0.35	0.72	0.64	0.34	0.81	0.72	0.53	0.30
Er	0.91	2.00	1.90	0.95	2.50	2.00	1.55	1.00
Tm	0.13	0.30	0.28	0.14	0.33	0.29	0.22	0.16
Yb	0.76	1.82	1.83	0.87	2.20	1.75	1.26	1.09
Lu	0.12	0.27	0.27	0.12	0.33	0.26	0.19	0.17

; SMC = Southern Domain

Ce83-77 SMC	Vp83-79 SMC	Pey83-82 SMC	BR 6 SMC	BR 9 SMC	BR 12 SMC	Ms 15 SMC	AL 851 SMC	AL 852 SMC
0.02	0.03	0.08	0.03	0.09		0.05	0.92	5.18
0.16	0.14	1.53	0.17	4.82		0.27	10.53	61.10
0.03	0.57	0.27	0.38	0.75	0.01	1.02	0.39	0.76
0.15	0.19	0.23	0.09	0.51	0.00	0.25	0.07	0.23
2.14	7.79	3.93	4.73	2.81	0.09	6.89	5.06	22.79
0.01	0.06	0.02	0.07	0.02	0.02	0.04	0.07	0.25
0.16	3.26	3.01	2.20	13.53	0.74	11.28	1.78	11.45
0.99	8.70	2.98	4.36	15.81	3.25	21.08	4.91	31.70
0.18	0.40	0.55	0.71	0.64	0.04	0.58	0.87	4.18
0.27	1.41	0.62	0.81	1.18	0.63	1.84	0.81	4.46
24.2	125.6	53.6	36.2	104.2	67.0	158.0	74.3	179.3
2.14	7.79	3.93	4.73	2.81	3.80	6.89	5.06	22.79
13.14	48.03	26.51	32.58	4.11	29.80	21.79	40.93	88.52
0.61	1.41	0.77	1.17	0.18	0.86	0.62	1.55	2.54
1.05	2.20	1.62	2.06	0.31	1.54	1.37	1.78	4.23
0.49	0.88	0.66	0.83	0.11	0.62	0.51	0.72	1.52
1.57	3.28	2.57	2.63	0.32	2.20	1.32	2.03	3.14
0.34	0.47	0.41	0.52	0.07	0.44	0.30	0.49	0.63
2.36	3.29	3.28	3.98	0.47	2.94	2.09	3.70	3.85
12.52	16.98	17.40	19.94	2.46	19.20	12.48	22.65	21.12
0.52	0.67	0.75	0.84	0.10	0.67	0.45	0.83	0.81
1.44	1.87	2.13	2.56	0.30	1.95	1.31	2.54	2.32
0.23	0.27	0.29	0.34	0.05	0.28	0.18	0.36	0.34
1.48	1.81	2.07	2.42	0.36	1.85	1.09	2.29	1.98
0.24	0.25	0.30	0.30	0.07	0.27	0.17	0.35	0.30

Z4	Z 7	Z 8	Z 10	Z 28	Z 42	RP83-72	RP87-2	RP91-20
SMC	SMC	SMC	SMC	SMC	SMC	SMC	SMC	SMC
1.50	0.09	0.05	0.04		0.04			
56.93	1.16	0.35	0.26		0.26			
3.24	2.21	0.17	0.82	0.72	0.34	2.80	0.02	0.02
3.96	0.58	0.09	0.66	0.33	0.09	0.51	0.02	0.02
8.72	6.99	3.53	0.27	0.13	6.10	0.15	0.05	0.08
0.06	0.01	0.04	0.02	0.01	0.06	0.03	0.02	0.02
34.94	28.37	12.14	5.96	3.80	2.26	20.00	0.34	0.12
39.09	34.37	19.20	3.98	3.70	6.01	58.00	2.35	1.11
6.65	0.72	0.47	1.46	0.67	1.15	0.67	0.18	0.70
3.33	2.68	1.49	0.20	0.07	1.03	6.70	0.62	0.34
174.5	282.5	98.5	24.4	20.7	57.2	353.0	49.0	24.0
8.72	6.99	3.53	0.27	0.42	6.10	22.00	3.61	2.50
15.61	0.22	2.76	0.18	0.07	38.68	22.00	25.00	16.50
1.20	0.03	0.08	0.05	0.01	1.63	0.70	0.87	0.71
1.34	0.53	0.44	0.11	0.18	2.26	3.10	1.69	1.39
0.61	0.21	0.19	0.05	0.06	1.02	0.82	0.76	0.53
6.21	0.63	0.83	0.48	0.41	3.42	2.10	2.30	1.94
0.55	0.06	0.13	0.10	0.10	0.69	0.32	0.46	0.42
3.84	0.48	0.99	1.00	0.97	5.23	1.80	2.90	2.80
11.95	3.65	6.19	6.95	7.00	23.28	10.00	19.30	18.40
0.96	0.12	0.23	0.29	0.23	1.19	0.35	0.72	0.64
3.26	0.39	0.74	0.91	0.78	3.21	0.91	2.00	1.90
0.50	0.06	0.12	0.15	0.12	0.45	0.13	0.30	0.28
3.92	0.46	0.84	1.02	0.92	3.06	0.76	1.82	1.83
0.40	0.07	0.12	0.14	0.12	0.45	0.12	0.27	0.27

BO83-74	**Ta 7**	**Ta 13**	**Ta 19**	**Gr83-75**	**Ce83-77**	**Vp83-79**	**Pey83-82**	**BR 6**
SMC	**SMC**	**SMC**	**SMC**	**SMC**	**SMC**	**SMC**	**SMC**	**SMC**
0.01		0.03	0.02	0.02	0.02	0.03	0.08	0.03
0.05		0.31	0.27	0.09	0.16	0.14	1.53	0.17
0.02	0.90	0.56	0.74	0.05	0.03	0.57	0.27	0.38
0.01	0.24	0.27	0.21	0.02	0.15	0.19	0.23	0.09
2.17	0.70	8.86	7.49	2.42	2.14	7.79	3.93	4.73
0.04	0.02	0.01	0.09	0.04	0.01	0.06	0.02	0.07
0.65	6.70	1.84	11.42	1.12	0.16	3.26	3.01	2.20
2.08	7.20	5.69	19.67	3.39	0.99	8.70	2.98	4.36
0.12	1.20	0.49	0.31	0.24	0.18	0.40	0.55	0.71
0.36	0.90	0.68	2.78	0.53	0.27	1.41	0.62	0.81
28.7	103.0	55.7	240.4	24.7	24.2	125.6	53.6	36.2
2.17	4.30	8.86	7.49	2.42	2.14	7.79	3.93	4.73
14.16	40.00	31.54	39.07	14.10	13.14	48.03	26.51	32.58
0.43	1.31	1.00	0.89	0.40	0.61	1.41	0.77	1.17
0.89	2.00	1.68	2.06	0.77	1.05	2.20	1.62	2.06
0.33	0.67	0.66	0.69	0.28	0.49	0.88	0.66	0.83
0.77	2.80	1.37	1.40	0.75	1.57	3.28	2.57	2.63
0.20	0.54	0.44	0.39	0.18	0.34	0.47	0.41	0.52
1.51	3.70	3.29	2.63	1.41	2.36	3.29	3.28	3.98
8.78	23.00	29.94	11.87	9.25	12.52	16.98	17.40	19.94
0.34	0.81	0.72	0.53	0.30	0.52	0.67	0.75	0.84
0.95	2.50	2.00	1.55	1.00	1.44	1.87	2.13	2.56
0.14	0.33	0.29	0.22	0.16	0.23	0.27	0.29	0.34
0.87	2.20	1.75	1.26	1.09	1.48	1.81	2.07	2.42
0.12	0.33	0.26	0.19	0.17	0.24	0.25	0.30	0.30

BR 9	**Mb 1**	**Mb 8**	**Mb 9**	**Mb 36**	**Mb 47**	**Mb 50**	**Mb 57**	**Bt 1**
SMC	**NMC**	**NMC**	**NMC**	**NMC**	**NMC**	**NMC**	**NMC**	**NMC**
0.09		0.62	0.01	0.02				
4.82		25.85	0.29	0.15				
0.75	2.34	5.39	0.07	0.02	0.10	0.03	3.10	0.23
0.51	1.20	1.03	0.55	0.02	0.68	0.27	0.93	0.07
2.81	0.01	5.35	0.04	0.01	0.36	0.01	0.01	0.16
0.02	0.01	0.01	0.02	0.00	0.02	0.01	0.01	0.01
13.53	42.40	27.36	5.24	0.16	3.01	2.90	49.87	3.10
15.81	24.93	31.96	0.70	0.04	0.42	0.59	71.10	9.70
0.64	1.05	0.90	0.59	0.19	0.59	0.36	0.99	1.00
1.18	0.51	2.16	0.01	0.01	0.02	0.01	2.93	1.18
104.2	454.0	768.6	64.0	9.6	53.3	30.1	468.7	355.0
2.81	0.49	5.35	0.04	0.01	0.08	0.04	3.85	4.70
4.11	0.02	0.16	0.12	0.02	0.15	0.01	3.01	12.10
0.18	0.02	0.06	0.04	0.04	0.15	0.02	0.13	0.24
0.31	0.07	0.27	0.10	0.07	0.19	0.07	0.27	1.04
0.11	0.03	0.11	0.09	0.03	0.08	0.03	0.10	0.32
0.32	0.25	0.39	0.41	0.18	0.65	0.34	0.36	0.75
0.07	0.06	0.05	0.09	0.04	0.12	0.07	0.07	0.12
0.47	0.60	0.47	0.94	0.43	1.23	0.87	0.50	0.72
2.46	4.40	3.33	5.92	2.81	6.80	6.40	3.27	4.80
0.10	0.14	0.10	0.22	0.10	0.29	0.22	0.11	0.16
0.30	0.52	0.39	0.76	0.34	0.88	0.75	0.38	0.50
0.05	0.08	0.07	0.11	0.05	0.21	0.11	0.05	0.08
0.36	0.59	0.54	0.90	0.40	1.10	0.85	0.44	0.59
0.07	0.08	0.08	0.13	0.05	0.11	0.12	0.06	0.09

Bt 3 NMC	Bt 11 NMC	Bt 14 NMC	Bt 19 NMC	Bt 27 NMC	Bt 39 NMC	Bt 40 NMC	FR 9 NMC	FR 10 NMC
0.13	0.02	0.03	0.07	0.01			11.13	
0.14	0.20	1.03	0.80	0.02			82.13	
0.13	0.02	0.26	0.28	0.05	0.56	0.28	0.82	0.05
0.12	0.02	0.05	0.03	0.02	0.13	0.08	0.37	0.04
0.64	1.78	6.69	2.23	0.56	1.50	0.05	1.26	0.24
0.01	0.01		0.04	0.00	0.19	0.01	0.07	0.02
1.28	0.73	2.36	3.15	0.44	4.83	3.20	2.79	1.13
1.77	2.40	8.11	6.03	1.11	11.70	8.50	3.62	3.40
0.33	1.21	0.09	0.83	0.96	0.40	0.28	2.43	0.10
0.17	0.39	1.40	0.60	0.14	1.36	1.21	0.34	0.62
31.8	417.7	290.0	340.6	40.8	99.0	46.0	12.4	34.2
0.64	1.78	6.69	2.23	0.56	5.19	5.90	1.26	3.60
1.12	10.26	5.75	3.59	1.36	19.00	41.00	63.70	26.30
0.05	0.39	0.14	0.13	0.06	0.44	1.33	1.14	0.32
0.19	0.42	1.54	0.32	0.23	1.03	1.89	0.26	0.89
0.08	0.20	0.51	0.19	0.09	0.34	0.67	0.13	0.28
0.27	0.46	1.19	0.44	0.41	1.20	2.19	0.26	0.70
0.06	0.07	0.15	0.09	0.09	0.25	0.41	0.05	0.10
0.48	0.50	0.83	0.62	0.74	1.65	2.50	0.45	0.62
2.95	3.22	4.29	3.66	4.12	11.50	15.60	4.19	3.50
0.11	0.11	0.16	0.13	0.18	0.41	0.54	0.13	0.12
0.39	0.38	0.43	0.45	0.51	1.24	1.56	0.49	0.35
0.06	0.07	0.07	0.07	0.08	0.18	0.21	0.08	0.05
0.46	0.46	0.38	0.53	0.55	1.21	1.38	0.56	0.42
0.07	0.07	0.06	0.08	0.08	0.19	0.20	0.10	0.06

FR 11 NMC	ST 2 NMC	CH 11 NMC
	0.02	
	0.23	
0.86	3.25	0.15
0.37	1.05	0.12
0.87	1.11	0.01
0.03	0.01	0.03
6.60	38.17	1.94
14.10	61.86	1.71
0.16	0.35	0.31
1.46	0.27	0.13
56.6	306.4	17.7
5.95	1.11	0.73
26.50	0.09	3.73
0.35	0.04	0.18
1.11	0.15	0.46
0.35	0.08	0.20
0.84	0.34	0.93
0.12	0.13	0.17
0.78	1.16	1.39
4.10	27.95	8.82
0.14	0.30	0.30
0.39	0.92	0.94
0.06	0.14	0.13
0.48	0.89	0.92
0.07	0.15	0.12

Table 2. Trace elements in clinopyroxenes from Lower Silesia (Poland), analysed by LA-ICP-MS.

element	**LA74**	**LA 56**	**LA 62**	**LA 81**	**LA 31**	**LA 58**	**LA 39**	**LA 85**
Rb	0.03	0.04	0.10	0.07	0.06	0.25	0.07	0.02
Ba	0.22	0.22	1.62	0.85	0.13	0.13	0.43	0.10
Th	1.51	2.38	0.52	1.82	0.74	0.93	0.56	1.26
U	0.41	0.47	0.15	0.33	0.19	0.26	0.15	0.39
Nb	14.99	2.64	5.87	4.55	2.12	14.21	0.40	3.94
Ta	0.06	0.05	0.02	0.04	0.00	0.10	0.00	0.02
La	21.14	9.55	6.06	14.04	8.42	12.54	4.08	11.89
Ce	48.00	12.34	15.64	18.09	14.54	30.80	4.59	18.15
Pb	0.46	0.62	0.24	0.35	0.48	0.47	0.35	0.34
Pr	4.93	0.96	1.64	1.43	1.05	3.54	0.22	1.43
Sr	220.5	58.4	176.8	179.2	101.3	402.8	25.9	122.7
Nd	14.99	2.64	5.87	4.55	2.12	14.21	0.40	3.94
Zr	2.67	0.48	5.15	15.25	0.18	15.98	0.14	0.59
Hf	0.08	0.08	0.15	0.48	0.04	0.16	0.05	0.02
Sm	1.49	0.38	0.94	0.82	0.12	2.41	0.08	0.31
Eu	0.37	0.15	0.25	0.26	0.04	0.69	0.04	0.10
Gd	0.89	0.79	0.72	0.73	0.24	1.99	0.26	0.38
Tb	0.16	0.17	0.10	0.10	0.05	0.23	0.08	0.08
Dy	1.14	1.54	0.61	0.66	0.56	1.41	0.81	0.65
Y	6.90	8.49	3.47	3.76	4.38	6.69	5.98	4.98
Ho	0.28	0.32	0.12	0.14	0.14	0.24	0.23	0.16
Er	0.90	1.09	0.37	0.39	0.46	0.69	0.78	0.55
Tm	0.14	0.16	0.05	0.06	0.09	0.09	0.12	0.08
Yb	0.92	0.99	0.36	0.38	0.64	0.66	0.82	0.66
Lu	0.17	0.15	0.05	0.05	0.09	0.09	0.13	0.10

LA 83	LA 38	WG 10	Tr 27	LU 50	LU 28	LU 8	LA 67	LA74
0.34	0.05	0.12	0.05	0.04	0.05	0.02	0.33	0.03
0.96	0.28	0.09	0.29	0.26	0.14	0.05	0.10	0.22
0.70	0.26	0.13	0.48	0.24	0.56	0.94	0.85	1.51
0.32	0.14	0.05	0.10	0.07	0.13	0.19	0.26	0.41
2.35	0.57	21.58	24.96	13.93	7.30	11.28	8.89	14.99
0.09	0.01	0.16	0.08	0.04	0.08	0.03	0.10	0.06
8.11	5.95	6.41	10.35	6.43	6.52	11.04	9.43	21.14
12.82	7.23	24.90	32.94	19.45	14.78	27.09	19.40	48.00
0.50	0.28	0.15	0.57	0.20	0.29	0.60	0.79	0.46
1.15	0.33	4.31	5.14	2.99	1.81	3.06	2.17	4.93
57.4	37.8	183.0	368.5	217.1	240.9	445.9	91.9	220.5
2.35	0.57	21.58	24.96	13.93	7.30	11.28	8.89	14.99
1.13	0.58	51.48	138.47	86.29	12.15	7.66	15.52	2.67
0.35	0.02	1.24	2.57	0.97	0.08	0.22	0.20	0.08
0.60	0.13	5.09	6.47	3.12	1.52	1.64	1.35	1.49
0.23	0.02	1.43	2.00	0.99	0.46	0.51	0.39	0.37
1.50	0.14	4.10	5.91	2.47	1.26	1.07	1.21	0.89
0.25	0.05	0.50	0.76	0.35	0.17	0.14	0.18	0.16
1.60	0.28	2.90	5.05	1.99	0.96	0.76	1.14	1.14
11.21	2.25	10.93	22.15	9.04	4.52	3.38	6.32	6.90
0.28	0.08	0.48	0.88	0.35	0.17	0.13	0.20	0.28
1.04	0.24	1.06	2.23	0.90	0.44	0.39	0.60	0.90
0.17	0.06	0.13	0.29	0.11	0.06	0.05	0.09	0.14
0.76	0.34	0.78	1.85	0.65	0.37	0.41	0.66	0.92
0.17	0.09	0.09	0.26	0.08	0.05	0.06	0.08	0.17

LA 56	**LA 62**	**LA 81**	**LA 31**	**LA 58**	**LA 39**	**LA 85**
0.04	0.10	0.07	0.06	0.25	0.07	0.02
0.22	1.62	0.85	0.13	0.13	0.43	0.10
2.38	0.52	1.82	0.74	0.93	0.56	1.26
0.47	0.15	0.33	0.19	0.26	0.15	0.39
2.64	5.87	4.55	2.12	14.21	0.40	3.94
0.05	0.02	0.04	0.00	0.10	0.00	0.02
9.55	6.06	14.04	8.42	12.54	4.08	11.89
12.34	15.64	18.09	14.54	30.80	4.59	18.15
0.62	0.24	0.35	0.48	0.47	0.35	0.34
0.96	1.64	1.43	1.05	3.54	0.22	1.43
58.4	176.8	179.2	101.3	402.8	25.9	122.7
2.64	5.87	4.55	2.12	14.21	0.40	3.94
0.48	5.15	15.25	0.18	15.98	0.14	0.59
0.08	0.15	0.48	0.04	0.16	0.05	0.02
0.38	0.94	0.82	0.12	2.41	0.08	0.31
0.15	0.25	0.26	0.04	0.69	0.04	0.10
0.79	0.72	0.73	0.24	1.99	0.26	0.38
0.17	0.10	0.10	0.05	0.23	0.08	0.08
1.54	0.61	0.66	0.56	1.41	0.81	0.65
8.49	3.47	3.76	4.38	6.69	5.98	4.98
0.32	0.12	0.14	0.14	0.24	0.23	0.16
1.09	0.37	0.39	0.46	0.69	0.78	0.55
0.16	0.05	0.06	0.09	0.09	0.12	0.08
0.99	0.36	0.38	0.64	0.66	0.82	0.66
0.15	0.05	0.05	0.09	0.09	0.13	0.10